The Journal of Chemical Physics

RESEARCH ARTICLE | JULY 06 2023

Mass spectroscopy study of the intermediate magic-size cluster species during cooperative cation exchange

Special Collection: 40 Years of Colloidal Nanocrystals in JCP

Yuan Yao ; Reilly Lynch ; Richard D. Robinson

J. Chem. Phys. 159, 014704 (2023)
https://doi.org/10.1063/5.0151904

The Journal of Chemical Physics ARTICLE scitation.org/journal/jcp

Mass spectroscopy study of the intermediate magic-size cluster species during cooperative cation exchange

Cite as: J. Chem. Phys. 159, 014704 (2023); doi: 10.1063/5.0151904
Submitted: 25 March 2023 • Accepted: 2 June 2023 •
Published Online: 6 July 2023

Yuan Yao,[1] Reilly Lynch,[1] and Richard D. Robinson[1,2,a)]

AFFILIATIONS

[1] Department of Materials Science and Engineering, Cornell University, Ithaca, New York 14853, USA
[2] Kavli Institute at Cornell for Nanoscale Science, Ithaca, New York 14853, USA

Note: This paper is part of the JCP Special Topic on 40 Years of Colloidal Nanocrystals in JCP.
[a)] **Author to whom correspondence should be addressed:** rdr82@cornell.edu

ABSTRACT

Cation exchange is a versatile post-synthetic method to explore a wide range of nanoparticle compositions, phases, and morphologies. Recently, several studies have expanded the scope of cation exchange to magic-size clusters (MSCs). Mechanistic studies indicated that MSC cation exchange undergoes a two-stage reaction pathway instead of the continuous diffusion-controlled mechanism found in nanoparticle cation exchange reactions. The cation exchange intermediate, however, has not been well-identified despite it being the key to understanding the reaction mechanism. Only indirect evidence, such as exciton peak shifts and powder x-ray diffraction, has been used to indicate the formation of the cation exchange intermediate. In this paper, we investigate the unusual nature of cation exchange in nanoclusters using our previously reported CdS MSC. High-resolution mass spectra reveal two cation exchanged reaction intermediates [$Ag_2Cd_{32}S_{33}$(L) and $AgCd_{33}S_{33}$(L), L: oleic acid] as well as the fully exchanged Ag_2S cluster. Crystal and electronic structure characterizations also confirm the two-stage reaction mechanism. Additionally, we investigate the Cu/CdS MSC cation exchange reaction and find a similar two-stage reaction mechanism. Our study shows that the formation of dilutely exchanged intermediate clusters can be generally found in the first stage of the MSC cation exchange reaction. By exchanging different cations, these intermediate clusters can access varying properties compared to their unexchanged counterparts.

INTRODUCTION

Louis Brus' early papers on the synthesis and properties of semiconductor nanoparticles laid the foundation for the nanoparticle community by demonstrating the unique physical and chemical properties of these materials.[1–3] At the present time, this field has expanded significantly with a diverse range of material compositions, properties, and sizes (including the smaller nanocluster systems) and has become an essential part of many scientific and engineering disciplines. The cation exchange reaction has been developed as a versatile post-synthetic method to explore a wide range of nanoparticle compositions, phases, and morphologies.[4,5] Previous mechanistic studies report that the nanoparticle cation exchange is initiated by shell atom symmetry breaking and recrystallization, followed by diffusion and a controlled cation exchange process.[6,7] Several studies have focused on the cation exchange of magic-size clusters (MSCs) to create MSCs with a wide range of compositions.[8–13] Mechanistic studies of cation exchange on MSCs and small nanocrystals indicate that the reaction undergoes a non-diffusional two-stage process. At stage one, a small number of cations are exchanged and form a metastable MSC intermediate while preserving the original crystal structure.[2–5] Once the exchanged cation reaches critical concentration, the MSC intermediate undergoes an avalanche cation exchange reaction, rapidly forming the fully exchanged product. This mechanism was first demonstrated by White *et al.* in small CdSe nanocrystals with ~1000 atoms.[8] In this report, the Cu/CdSe MSC cation exchange starts with the slow exchange of 1–3 Cu atoms, forming an intermediate phase, followed by an avalanche reaction, which forms completely exchanged Cu_2Se MSCs.[8] These intermediate forms, however, have not been well identified, despite them being the key to understanding the reaction mechanism. Indirect evidence, such as exciton peak

shifts and crystal structure changes based on powder x-ray diffraction characterization, has been used to indicate the formation of the cation exchange intermediate.[9] Single-crystal x-ray diffraction is the most reliable method to provide the precise crystal structure of nanoclusters,[14] but growing MSC single crystals are hindered by the long alkyl chain surface ligand, and only a few successful attempts have been reported by using rigid ligands.[15,16] Some successes have been made on MSC atomic composition using high-resolution matrix-assisted laser desorption/ionization-time of flight (MALDI-TOF) mass spectroscopy. MALDI-TOF mass spectrometry is a widely used method to identify nanoclusters as well as their doped derivatives based on the characteristic isotope distribution.[12,17,18] Employing MALDI-TOF mass spectroscopy, one may directly observe the changes in the magic-size clusters at the molecular level throughout the cation exchange process.

In this paper, we investigate the unusual nature of cation exchange in nanoclusters using our previously reported CdS MSC.[19] MALDI-TOF mass spectroscopy results reveal two cation exchanged reaction intermediates [$Ag_2Cd_{32}S_{33}$(L) and $AgCd_{33}S_{33}$(L), L: oleic acid] when 50% Ag is added. Once the Ag addition exceeds 50%, fully exchanged Ag_2S nanoclusters appear. This rapid transition from a one to two-atom doped MSC to a fully exchanged Ag_2S nanocluster indicates an avalanche reaction is triggered at a critical Ag concentration, which leads to the rapid restriction to a fully exchanged Ag_2S nanocluster. Additional optical and structural characterizations agree with the proposed two-stage reaction mechanism. Kinetic studies show the formation of CdS MSC intermediates and Ag_2S, and the conversion to both follows first-order kinetic. Based on our mechanistic study, we construct a quantitative relationship between Ag addition and the cation exchange reaction product. With the correlation between Ag addition and cation exchange products, we synthesize and isolate dilutely Ag exchanged CdS MSC intermediate with a precise number of Ag atoms [$Ag_2Cd_{32}S_{33}$(L)]. Additionally, we show that this two-stage reaction mechanism also applies to Cu cation exchange in CdS MSC and potentially is general to other MSC cation exchange reactions.

RESULTS AND DISCUSSION

To study the MSC cation exchange reaction mechanism, a series of Ag/CdS MSC cation exchange reactions are conducted (experimental details in the supplementary material). Inductively coupled plasma-optical emission spectrometry (ICP-OES) is used to characterize the amount of Ag that is incorporated into the CdS MSC [Fig. 1(a), details shown in the supplementary material). Initially, from 0 to a 75% Ag addition $\left(\frac{Moles_{Ag}}{Moles_{Cd}}\%\right)$, the Ag% incorporation increases from 0% to 8.0%. Past this point, as Ag is added from 75% to 135%, there is a rapid increase in Ag% incorporation (8.0%–40.4%). In this range, the Ag incorporation is greater by a factor of 5.1 times compared to the first Ag addition stage (0%–75% added). To quantify the Ag incorporation rate in the first and second regions, the Ag incorporation vs addition curve is linearly fit between 0% to 75% and 100% to 135%. The fitted slopes $L_1 = 0.11$ and $L_2 = 0.83$ indicate that the Ag incorporation rate in the second region is 7.5 times higher than in the first region. In the final stage, as the Ag addition increases from 135% to 175%, the Ag incorporation plateaus at ~40%, indicating the cation exchange reaction has already completed at 135% Ag addition.

At the face of it, a 40% substitution of Cd for Ag is substoichiometric and implies that the reaction has not been completed and a residual core of CdS or unreacted CdS clusters/fragments remains. We hypothesize that this significant excess of unreacted Cd is contributed not from the MSCs but from local $Cd(oleate)_2$ trapped in the mesophase. To test our hypothesis, we conduct a size-selective precipitation experiment on an Ag exchanged sample (100% Ag addition). Because the $Cd(oleate)_2$ is a much smaller molecule compared to the CdS MSC, we should be able to vary its precipitation by controlling the antisolvent (acetone) to solvent (toluene) ratio (experimental details shown in the supplementary material). The results of our experiment show that the silver concentration in the precipitated product (Ag% incorporation, measured from ICP, Fig. S1) decreases from 31.6% to 12.1% as we increase the antisolvent to solvent ratio from one to five. The decrease in Ag% measured is due to increased $Cd(oleate)_2$ precipitation as we increase the antisolvent to solvent ratio. Our size-selective precipitation experiment proves $Cd(oleate)_2$ does contribute to the Cd content measured in ICP. In order to preserve consistent results between cation exchange samples with respect to their $Cd(oleate)_2$ ratio, we use a constant antisolvent/solvent ratio for our sample wash (details in the supplementary material). Inevitably, this leads to the overestimation of the Cd content in our product. Nevertheless, we hold the view that these errors exhibit consistency between samples, thereby establishing a background level against which the variations can be accurately ascertained.

Ex-situ UV–Vis absorption spectroscopy finds that as the Ag content increases the changes to the excitonic feature can be divided into two stages [Fig. 1(b)]. In the first stage, the exciton peak gradually shifts from 324 to 327 nm as the Ag content increases to 4.0%. In the second stage, further Ag content increases lead to the reduction in the 327 nm exciton peak intensity, which completely diminishes at an Ag content of 40.4%. As a control experiment, we inject the same amount of solvent without Ag, and no change in the exciton peak is observed (Fig. S2). The small shift in the exciton feature in stage 1 indicates a slight change in the CdS MSC electronic structure possibly due to the incorporation of a few Ag atoms in the CdS MSC. In the second stage, the reduction in the exciton peak intensity indicates that the CdS MSC starts to transform into a product with a completely different electronic structure. Our two-stage UV–Vis results are consistent with previously reported CdSe MSC cation exchange with Cu.[9]

In-situ UV–Vis absorption spectroscopy of the 100% Ag addition (12.1% Ag incorporation) reveals that the reaction dynamics can be divided into two distinct regions (Fig. 2). Within the first 20 s of the Ag addition, the exciton peak shifts from 324 to 327 nm, accompanied by a rapid decrease in the peak absorbance (decreases from 0.9 to 0.3) [Fig. 2(a)]. Between 20 and 100 s of the reaction, the peak absorbance decreases to 0.07. The final absorbance change in the kinetic study is consistent with the 100% Ag addition case shown in Fig. 1, where absorbance significantly reduces from 1.37 to 0.23 after Ag addition. Based on the Beer–Lambert law, the peak absorbance is linearly correlated with the CdS MSC solution concentration and can be used as an indicator of the reaction progress. Thus, fitting the time-dependent peak absorbance reveals the kinetics of the cation exchange reaction [Fig. 2(b)]. A recent study

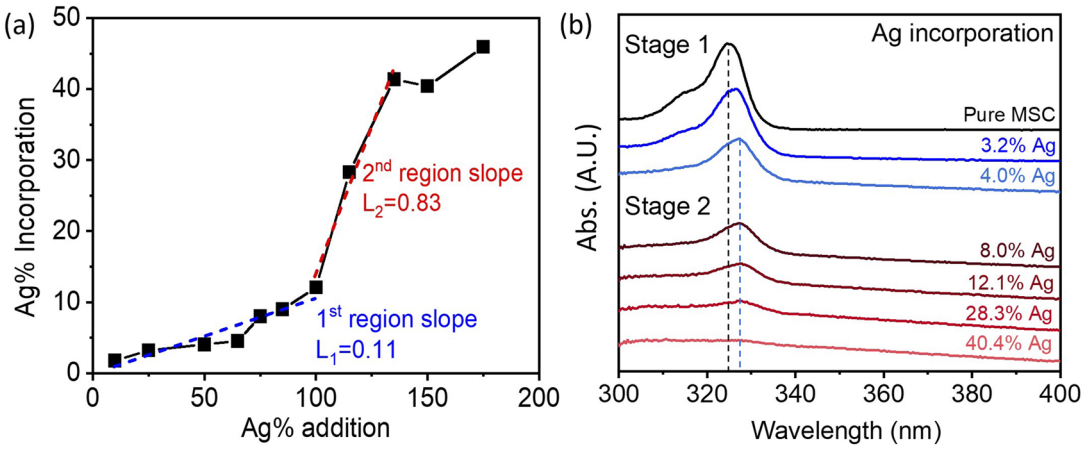

FIG. 1. Composition and UV–Vis absorption analysis of the cation exchange reaction of CdS MSCs with Ag. (a) Silver addition plotted as a function of silver incorporation computed as $\left(\frac{Moles_{Ag}}{Moles_{Cd}}\%\right)$. The values for "Ag% addition" are determined from the ratio of the Ag precursor to CdS MSCs. The values for "Ag% incorporation" are determined from ICP data. As Ag addition increases from 0% to 75%, the fraction of Ag that is incorporated increases constantly up to ~8.0%. When 75%–135% Ag is added, a rapid increase in Ag incorporation occurs, starting at 8.0% and ending at 40.4%. The Ag incorporation vs addition curve is linearly fit between 0% to 75% and 100% to 135%. The fitted slopes, L_1 = 0.11 and L_2 = 0.83, indicate that in the second region the Ag incorporation is ~7.5 times faster compared to the first region. (b) Absorption spectra for samples with varying Ag incorporations. The exciton absorption peak displays two stages during the Ag content increase. Initially, as the Ag content increases up to 4.0%, the 324 nm exciton peak gradually shifts to 327 nm. Further increase in the Ag content then leads to continuous reduction in the absorbance peak, which completely diminishes when the Ag content reaches 40.4%.

has found that the cation exchange reaction for CdS into ZnS magic-size clusters follows first-order kinetics,[12] $\ln(A) = kt + I$, where A is the peak absorbance, k is the rate constant, t is the reaction time, and I is the initial absorbance. Attempting to fit our time-dependent absorption data (0–100 s) with a first-order fit (Fig. S3), however, results in a poor correlation especially in the timeframe of 0–20 s. Based on our previous finding of a two-stage reaction (Fig. 1), we tried fitting the time-dependent absorption data with first-order kinetics over two regions (0–20 s and 20–100 s). We found improved R^2 values in both regions [0.966 and 0.986, Fig. 2(b)]. Comparing the rate constants from the two stages, the rate constant extracted from the first stage (k = 0.056 for 0–20 s) is three times higher than that from the second stage (k = 0.019 for 20–100 s), further supporting the hypothesis that the cation exchange undergoes two reaction stages.

We examine the atomic structure and composition of the cation exchange reaction products using MALDI-TOF mass spectroscopy over a range of 3000–6000 m/z (Fig. 3). As the Ag% incorporation increases up to 8.0%, we observe the highest intensity peak at 5163 m/z, which shifts toward lower mass and a new peak around 4860 m/z [$Ag_2Cd_{32}S_{33}$] appears, which results from the removal of the oleic acid ligand. With further increases in Ag% incorporation, the peaks above 4500 m/z diminish and are replaced by new peaks in the 3200–4200 m/z region. Summarizing the evolution of

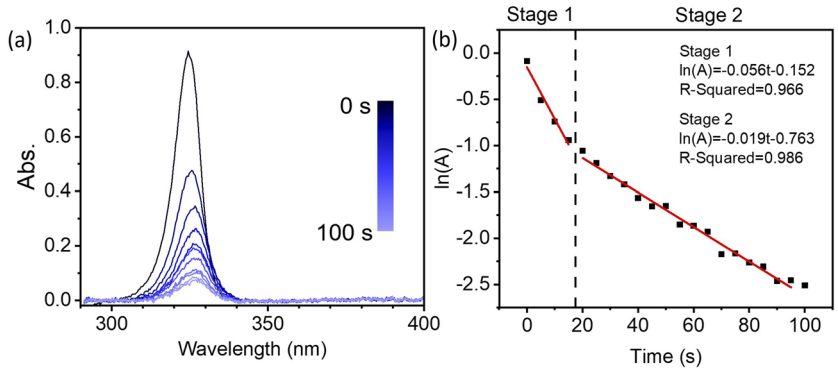

FIG. 2. *In-situ* UV–Vis absorption study on the Ag/CdS MSC cation exchange reaction with 100% Ag addition. (a) *In-situ* UV–Vis absorption from the cation exchange reaction after adding Ag to the CdS MSC at time 0. In the first 20 s after Ag addition, the exciton peak at 324 nm shifts to 327 nm accompanied by a rapid decrease in the exciton peak intensity from 0.9 to 0.3. Once the exciton peak is fully shifted to 327 nm, the absorbance slowly decreases and stabilizes at 0.07. (b) The time-dependent absorbance change is fitted in two separate regions (0–20 s and 20–100 s) with a first-order kinetic equation (inset). Both regions have strong R^2 fitting values (0.966 and 0.986).

the spectra, we see two reaction stages delineated by the 8.0% Ag incorporation point: (1) Below 8.0% Ag incorporation, the highest intensity peak at 5163 m/z shifts toward the lower mass. (2) Above 8.0% Ag incorporation, a group of peaks emerge between 3000 and 4000 m/z.

High-resolution MALDI-TOF is commonly used for nanocluster identification[10,11,13] by fitting the unique isotope mass distribution from each cluster. The native CdS MSC mass spectrum (MS) has four characteristic peaks above 5000 m/z corresponding to $Cd_{34}S_{33}(L)$ at 5163 m/z, $Cd_{36}S_{31}(L)$ at 5400 m/z, $Cd_{37}S_{32}(L)$ at 5549 m/z, and $Cd_{38}S_{33}(L)$ at 5694 m/z (L: oleic acid ligand, isotope fitting shown in Fig. S4). The peak at 5163 m/z [$Cd_{34}S_{33}(L)$] has the highest intensity and resolution; thus, it is used to monitor the change in the CdS MSC during Ag incorporation. Examination of the high-resolution MALDI-TOF MS around the 5163 m/z region reveals the highest intensity peak shifts from 5163 to 5159 m/z and then to 5155 m/z as the Ag content increases to 3.2% and then to 4.0% [Fig. 3(b)]. Isotope fitting finds that the decreased mass values correspond to the exchange of one and two Ag atoms with Cd [$AgCd_{33}S_{33}(L)$] and [$Ag_2Cd_{32}S_{33}(L)$]. These Ag exchanged clusters identified in MALDI-TOF are ligand stripped derivatives of the Ag exchanged clusters' intermediate. We name the two Ag exchanged cluster intermediates as the Ag–CdS and Ag_2–CdS MSC intermediate. Similarly, the mass region between 3200 and 4150 m/z can be examined as the silver content increases above 8.0% [Fig. 3(c)]. Below 8.0% Ag addition, the low intensity mass peaks in the spectra correspond to CdS cluster fragments (Fig. S5). At or above 8.0% Ag addition, a series of new peaks form in this region, which have short-range periodic mass differences of 32 m/z (e.g., 3297 vs 3329 m/z) and longer-range periodic mass differences of 248 m/z (e.g., 3297 vs 3545 m/z), corresponding to fragmentation of S and Ag_2S, respectively (Fig. S6). Isotope fitting of the peak pair between 3500 and 3600 m/z for the 28.3% sample shows the two peaks correspond to $Ag_{29}S_{13}$ and

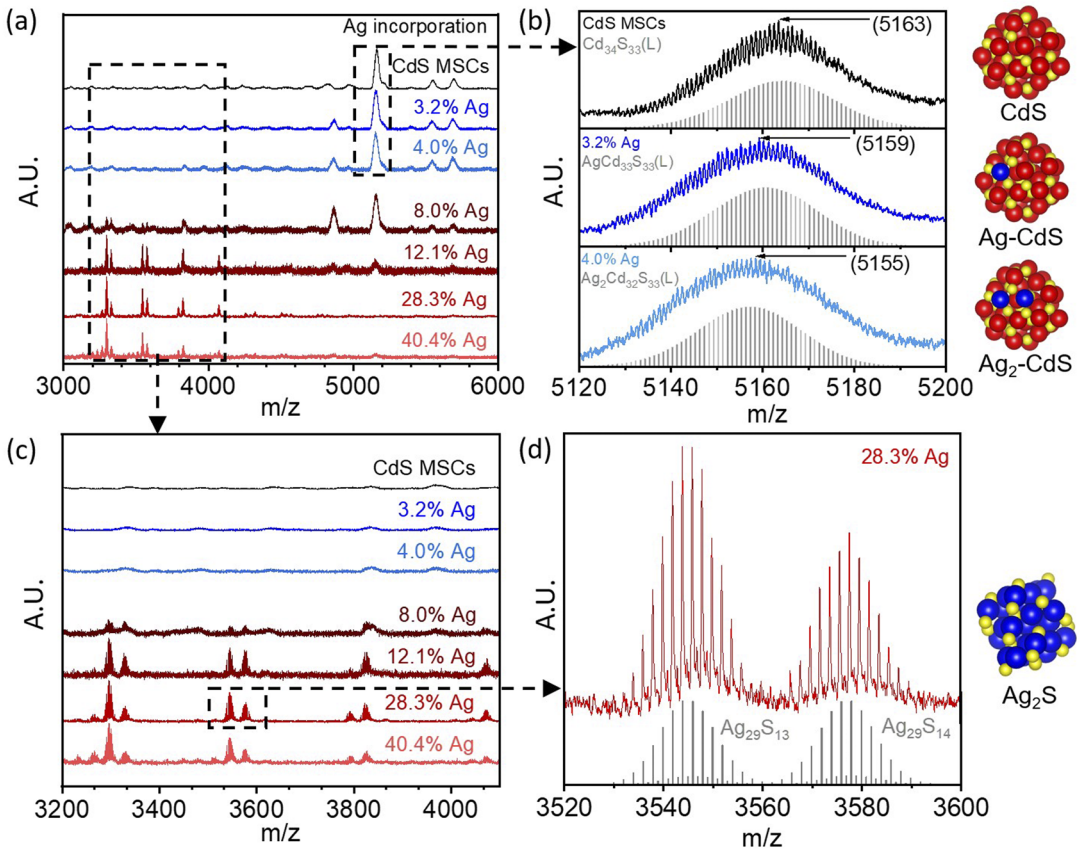

FIG. 3. *Ex-situ* MALDI-TOF MS studying the cation exchange intermediates and final product. (a) MS of samples that have undergone increasing levels of Ag incorporation (samples are measured post-exchange). Two m/z regions characterize the cation exchange process: (1) near the highest characteristic intensity peak at 5163 m/z and (2) between 3000 and 4000 m/z where a new group of peaks emerge when the Ag incorporation is above 8.0%. (b) High-resolution MS on the region between 5120 and 5200 m/z reveals the mass change during the first stage of the cation exchange reaction. As the Ag content increases to 3.2% and 4.0%, the most intense peak at 5163 m/z shifts lower to 5159 and 5155 m/z, which indicates one and two Ag atoms exchanging with Cd. The isotope distribution fittings are provided in the bar plot in the following. (c) High-resolution examination of the region between 3200 and 4150 m/z reveals mass changes that can be used to characterize the second stage of the cation exchange reaction. A series of periodic peaks between 3000 and 4000 m/z form as the silver content increase above 8.0%. Two periodic mass differences are observed: 32 m/z matches the atomic mass of the sulfur atom (e.g., 3297 vs 3329 m/z), and 248 m/z matches the molecular mass of Ag_2S (e.g., 3297 vs 3545 m/z). (d) Isotope fitting of one pair of the periodic mass peaks (28.3% Ag) between 3500 and 3600 m/z confirms they correspond to $Ag_{29}S_{13}$ and $Ag_{29}S_{14}$.

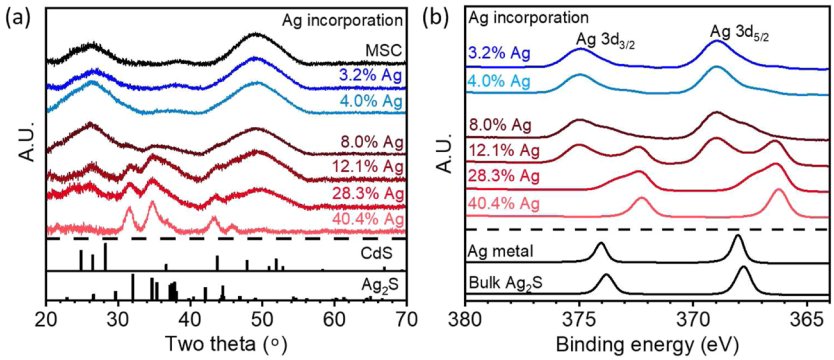

FIG. 4. *Ex-situ* XRD and XPS studying the crystal structure and electronic structure change during Ag cation exchange. (a) XRD analysis shows the crystal structure remains the same as the CdS phase until 4.0% Ag incorporation. At 8.0% Ag content, two small peaks between 30° to 40° emerge, which indicate the formation of the Ag_2S phase. Full exchange to Ag_2S is observed when Ag content reaches ~40.4%. (b) XPS results on the Ag 3d edge show the same binding energy ($3d_{3/2}$ at 374.9 eV and $3d_{5/2}$ at 368.9 eV) with Ag content up to 4.0%. As Ag content further increases, another set of doublets starts to form at lower binding energy ($3d_{3/2}$ at 372.3 eV and $3d_{5/2}$ at 366.3 eV) and coexists with the original peaks. When Ag content reaches 40.4%, the lower binding energy Ag doublets completely replace the original peaks.

$Ag_{29}S_{14}$, respectively [Fig. 3(d)]. Based on the above analysis, the new peaks between 3200 and 4150 m/z are Ag_2S cluster peaks.

To be noted, if we magnify the MS spectrum of fully exchanged sample (40.4% Ag addition), we observe periodic Ag_2S peaks up to ~6500 m/z (corresponding to $Ag_{53}S_{26}$, Fig. S7). Due to the potential fragmentation of larger Ag_2S clusters, the observed MS peaks only confirm the full conversion to Ag_2S clusters rather than quantifying of the cation exchange product.

The crystal structure evolution after Ag/CdS MSC cation exchange is studied by *ex-situ* x-ray diffraction [Fig. 4(a)]. The XRD spectra with up to 4.0% Ag incorporation show similar patterns with two broad peak centers at 26.3° and 49.1°, matching the CdS standard (PDF 00-006-0314). At 8.0% Ag incorporation, two peaks emerge between 30° and 40° and two other minor peaks between 40° and 45°, which rapidly increase in intensity as the Ag content increases. These new peaks completely replace the CdS peak when Ag content reaches 40.4%. The final phase at 40.4% Ag content matches the Ag_2S standard (PDF 01-080-8431) and confirms that the complete cation exchanged product is Ag_2S. Apart from the phase change, the XRD peaks also broaden as the Ag incorporation content increases, which indicates the nanocluster agglomerate during the cation exchange.

TABLE I. Summary of the reaction products with different amounts of Ag incorporation based on MALDI-TOF, XRD, and XPS data. All three characterization techniques converge to show that at or below 4.0% Ag content, the reaction products are dilutely exchanged Ag_2–CdS MSCs. Fully exchanged Ag_2S MSCs start to form between 4.0% and 8.0% Ag addition. At 40.4% Ag content, the Ag_2–CdS MSC intermediate has completely transformed to Ag_2S.

Silver incorporation	MALDI-TOF	XRD	XPS
0% Ag	CdS	CdS	CdS
3.2% Ag	CdS	CdS	CdS
4.0% Ag	CdS	CdS	CdS
8.0% Ag	CdS + Ag_2S	CdS + Ag_2S	CdS + Ag_2S
12.1% Ag	CdS + Ag_2S	CdS + Ag_2S	CdS + Ag_2S
28.3% Ag	Ag_2S	CdS + Ag_2S	CdS + Ag_2S
40.4% Ag	Ag_2S	Ag_2S	Ag_2S

X-ray photoemission spectroscopy (XPS) characterizes the electronic structure evolution during cation exchange by tracking the Ag 3d edge binding energy [Fig. 4(b)]. With up to 4.0% Ag incorporation, the Ag $3d_{3/2}$ and $3d_{5/2}$ binding energies remain constant at 374.9 and 368.9 eV, respectively. When the Ag content reaches 8.0%, we observe shoulders appearing at lower binding energy that grow into another set of doublets with binding energies at 372.3 eV ($3d_{3/2}$) and 366.3 eV ($3d_{5/2}$). When the silver content reaches 40.4%, only the peaks at 372.3 and 366.3 eV are present (fits in Fig. S9). XPS of Ag metal and bulk Ag_2S reference samples results in a $3d_{5/2}$ binding energy of 368.1 and 367.8 eV, respectively, which matches the literature reported values.[20–23] A significant 2.7 eV shift of the Ag 3d binding energy is observed between the Ag_2–CdS MSC intermediate (the CdS MSC doped with two Ag atoms; please see discussion around Fig. 3) and the fully exchanged Ag_2S. Due to the lack of reducing and oxidating agents, we assume the silver remains as Ag^+ through the cation exchange reaction. The literature has shown that

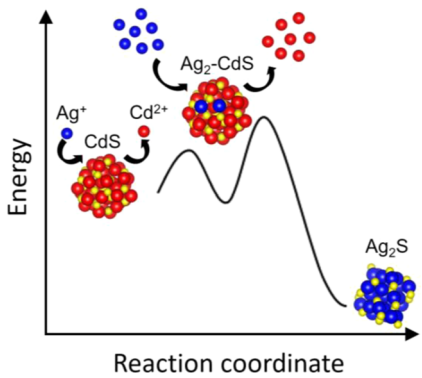

FIG. 5. Schematic of the two-stage CdS MSC cation exchange reaction with Ag^+. In stage 1, a stepwise exchange of 1–2 Ag atoms with Cd occurs and the CdS MSC crystal structure is retained. Once the cluster reaches a critical Ag concentration, an avalanche Ag cation exchange reaction occurs, resulting in a rapid transformation into Ag_2S.

the Ag^+ $3d_{5/2}$ binding energy can vary between 367.0 and 369.4 eV depending on the chemical environment,[24–26] and we propose that the different Ag chemical environments are the cause of the observed peak shifts. In the Ag_2–CdS MSC intermediate, Ag^+ ions are the minority in the system and are surrounded by the CdS nanocluster. Once the second stage of the cation exchange reaction is entered (e.g., 12.1% Ag incorporation sample), we observe two sets of doublets coexisting and corresponding to the intermediate stage where the Ag_2–CdS MSC intermediate has partially transformed into Ag_2S with Ag^+ ions sitting inside the Ag_2S nanocluster. In the fully exchanged sample, all the Ag^+ are within Ag_2S nanoclusters, and only one set of doublets with lower binding energy is observed.

The Cd 3d and S 2p XPS spectra are also collected and shown in the supplementary material (Fig. S10). Pure MSC Cd $3d_{3/2}$ and $3d_{5/2}$ peaks are located at 412.4 and 405.6 eV, respectively, which matches the reported values for a Cd–S bond.[25–27] Throughout the Ag addition series, there is no noticeable change in the Cd 3d peak [Fig. S10(a)]. Pure MSC sulfur $2p_{1/2}$ and $2p_{3/2}$ peaks are located at 162.8 and 161.6 eV, respectively [Fig. S10(b), Table S1]. As the Ag concentration increases to 8.0%, the doublets shift to a higher binding energy of 163.8 and 162.6 eV. Further addition of Ag up to 40.4% causes the S doublet to shift back to 162.8 and 161.6 eV. The 161.6 eV of S $2p_{3/2}$ binding energy matches the reported value for S^{2-} in either CdS or Ag_2S.[24,28] The increase in S binding energy in the 8.0% Ag addition sample can be assigned to S that is singly bonded to Ag (Ag–S–L, L corresponds to surface ligand)[27,29,30] or the presence of disulfide.[31] The presence of singly bonded S can be a result of the exposed nanocluster surface or fragments from the partial dissolution of the Ag_2–CdS MSC intermediate. This can be initiated by either the coordinating ligand trioctylphosphine (TOP) or more likely nitrate anions. After the Cd–S bond is cleaved, silver is able to bond with the free sulfur. Another nitrate is then able to cleave the remaining Cd–S bond and the cadmium nitrate leaves, likely reacting further with the TOP to form a metal complex.[32] This leaves the previously bonded sulfur exposed and unable to react due to the limited silver in the system (Fig. S11). Additionally, disulfide can form due to bond rearrangement during the partial dissolution of the Ag_2–CdS MSC intermediate.

Based on the *ex-situ* MALDI-TOF, XRD, and XPS results and analysis, we list the cation exchange products at different Ag incorporation values, and very consistent results are found (Table I). Juxtaposing the reaction products identified from the three characterization techniques, the 8.0% Ag sample stands out as the critical concentration at which Ag_2S starts to form. This finding is redundantly confirmed by these three characterization methods. At higher Ag concentrations, a discrepancy occurs at 28.3% Ag where the MALDI-TOF data indicates a full exchange to Ag_2S, but the XRD and XPS data still show some residual signal from the CdS MSCs. The lack of CdS MSC signal in the 28.3% Ag from MALDI-TOF is likely due to the fragmentation of the residual CdS MSCs.

Based on the above results, we propose a two-stage reaction for our Ag/CdS MSC cation exchange system. At stage 1, a stepwise substitution of Cd by Ag atoms leads to the formation of an Ag exchanged CdS MSC intermediate. From the MALDI-TOF and XRD results [Figs. 3(b) and 4(a)], the Ag_x-CdS intermediate contains up to two Ag atoms (Ag_2–CdS) and shares the same crystal structure as the unexchanged CdS MSC. After the Ag% incorporation reaches the critical concentration of 8.0%, MALDI-TOF and XRD results indicate that the Ag_2–CdS MSC intermediate starts to transform into Ag_2S (Fig. 5). The fact we are only able to observe up to two Ag atoms exchange into CdS MSCs indicates that further addition of Ag causes the CdS cluster fragmentation, followed by structural reorganization and Ag_2S cluster formation. Analogous two-stage reaction mechanisms can be found in both nanocluster and nanocrystal cation exchange process. For example, White *et al.* also found a two-stage reaction mechanism during their cation exchange of CdSe nanoclusters with Cu ions:[9] a lightly doped Cu/CdSe intermediate is identified by a shifted exciton peak, and increased Cu concentration triggers an avalanche cation exchange to Cu_2Se. Nelson *et al.* found the cation exchange of Cd with PbS nanocrystal is initiated by the symmetry breaking of the surface shell: amorphous rock salt CdS crystallizes into zinc blende CdS. After the complete

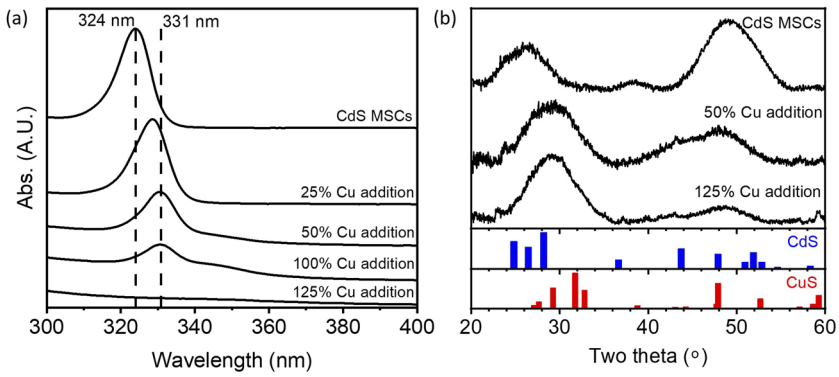

FIG. 6. Absorption and structural change throughout Cu/CdS MSC cation exchange. (a) The exciton absorption peak undergoes two stages of change as the Cu content increases. With up to 50% Cu addition, the 324 nm exciton peak shifts to 331 nm. Further addition of the Cu content up to 125% completely diminishes the exciton absorption peak. (b) XRD is used to probe the structure change at the 50% Cu addition (intermediate state) and 125% Cu addition (completely exchanged) samples. Pure CdS MSCs shows two wide peaks centered at at 26.3° and 49.0°. At 50% Cu addition, the original peaks shift to 29.1° and 47.9°. The 47.9° peak decreases in intensity relative to the peak at 29.1°. At 125% Cu addition, the two peaks remain at the same positions as the 50% addition case. Additionally, the peak at 48.9° further decreases in intensity. Two standards for CdS (PDF 00-006-0314) and CuS (JCPDS 6-464) are provided.

formation of the surface zinc blende CdS shell, the reaction proceeds through diffusion-controlled ion transport.[7] Our study provides detailed characterizations of the Ag_2–CdS MSC intermediate and final cation exchange product, which provide a deeper understanding of the cation exchange reaction mechanism in magic-size clusters.

To test the generality of the two-stage mechanism, we study the cation exchange of Cu with CdS MSCs (experimental details shown in the supplementary material). The exciton absorption and structural changes throughout the cation exchange process are shown in Fig. 6. Stepwise Cu ion addition leads to a similar exciton absorption peak shift as the Ag exchange case [Fig. 6(a)]. With up to 50% Cu addition, the exciton peak shifts from 324 to 331 nm, and the exciton peak intensity decreases to 36% of the original intensity. Further addition of Cu reduces the exciton peak intensity, which completely diminishes at 125% Cu addition. The *in-situ* UV–Vis Cu exchange experiment shows the time-dependent absorbance change can be fitted with first-order kinetic in two separate temporal regions (0–10 s and 10–90 s) (Fig. S12). The rate constant in the first stage is 14 times higher than the second stage (−0.15 vs −0.011), which matches the Ag exchange kinetic study.

The photoluminescence (PL) property of the Cu–CdS intermediate (50% addition) has changed significantly compared to the CdS MSC (Fig. S13). When excited at 285 nm, the pure MSC shows a single sharp PL peak at 330 nm. In comparison, the Cu–CdS intermediate shows a single peak center at 470 nm with an extended tail up to 800 nm. Our results match Hughes *et al.*'s report, which have shown that Cu doping in the CdSe/CdS core–shell nanoparticle gave rise to a broad longer wavelength PL peak. The red-shifted PL peak was attributed to the recombination of a delocalized conduction band electron with a hole created by copper doping.[33]

The crystal structures of the Cu–CdS intermediate sample (50% Cu addition) and fully exchanged sample (125% Cu addition) are analyzed by XRD and compared to unexchanged CdS MSCs (the parent clusters) [Fig. 6(b)]. The XRD spectrum of unexchanged CdS MSCs presents two broad peaks centered at 26.3° and 49.1°degrees, respectively. At 50% Cu addition, the two peaks shift to 29.1° and 47.9°, respectively. The complete Cu exchange sample retains a similar XRD pattern as the intermediate state, except for the peak at 47.9°, which is significantly decreased in intensity. Based on the CdS and CuS standards, both the intermediate and fully exchanged samples have a mixed structure between CdS (PDF 00-006-0314, zinc blende) and CuS (JCPDS 6-464, covellite). Additionally, unlike the fully exchanged Ag case where cluster aggregation is observed, the fully exchanged Cu case results in no cluster aggregation based on the similar width of the XRD peaks. Unfortunately, we are not able to directly observe the Cu–CdS intermediate cluster using MALDI-TOF MS most likely due to the structural instability when excited with high energy laser.

CONCLUSION

In this paper, we study the unusual cation exchange behavior of CdS MSCs with Ag. A two-stage reaction mechanism is confirmed by a series of optical, crystal structure, and electronic structure characterizations. At the first stage, dilute Ag is exchanged (up to 4.0% Ag incorporation), leading to the formation of Ag–CdS MSC intermediates. As the Ag incorporation content exceeds 8.0%, an avalanche reaction leads to the completely exchanged Ag_2S cluster formation. Most importantly, using high-resolution MALDI-TOF mass spectroscopy, we reveal two dilutely cation exchanged reaction intermediates [$Ag_2Cd_{32}S_{33}$(L) and $AgCd_{33}S_{33}$(L), L: oleic acid] as well as the fully exchanged Ag_2S. We construct a quantitative relationship between Ag addition and cation exchange reaction products based on our characterization results. Additionally, we investigate the Cu/CdS MSC cation exchange reaction and find a similar two-stage reaction mechanism. Our study shows the dilutely exchanged intermediate cluster can be generally found in the first stage of the MSC cation exchange reaction. By introducing different cations, these dilutely exchanged intermediate clusters can present varying properties compared to their unexchanged counterparts. Additionally, the dilutely exchanged clusters have the potential to be used as platforms for exchanging with other cations and potentially producing high entropy magic-size clusters.

SUPPLEMENTARY MATERIAL

The supplementary material contains additional experimental details for sample preparation, characterization methods, and figures.

ACKNOWLEDGMENTS

This work was supported in part by the National Science Foundation (NSF) under Award Nos. CMMI-2120947 and DMR-2003431. In addition, this work made use of the Cornell Center for Materials Research Shared Facilities, which are supported through the NSF MRSEC program (Grant No. DMR-1719875).

AUTHOR DECLARATIONS

Conflict of Interest

The authors have no conflicts to disclose.

Author Contributions

Yuan Yao: Conceptualization (equal); Data curation (equal); Formal analysis (equal); Investigation (equal); Methodology (equal); Project administration (equal); Resources (equal); Software (equal); Validation (equal); Visualization (equal); Writing – original draft (equal); Writing – review & editing (equal). **Reilly Lynch**: Formal analysis (equal); Investigation (equal); Resources (equal); Visualization (equal); Writing – review & editing (equal). **Richard D. Robinson**: Conceptualization (equal); Funding acquisition (equal); Methodology (equal); Project administration (equal); Resources (equal); Supervision (equal); Writing – original draft (equal).

DATA AVAILABILITY

The data that support the findings of this study are available within the article and its supplementary material.

REFERENCES

[1] L. E. Brus, "Electron–electron and electron-hole interactions in small semiconductor crystallites: The size dependence of the lowest excited electronic state," J. Chem. Phys. **80**(9), 4403–4409 (1984).

[2] L. Brus, "Electronic wave functions in semiconductor clusters: Experiment and theory," J. Phys. Chem. **90**(12), 2555–2560 (1986).

[3] L. E. Brus, "A simple model for the ionization potential, electron affinity, and aqueous redox potentials of small semiconductor crystallites," J. Chem. Phys. **79**(11), 5566–5571 (1983).

[4] B. J. Beberwyck, Y. Surendranath, and A. P. Alivisatos, "Cation exchange: A versatile tool for nanomaterials synthesis," J. Phys. Chem. C **117**(39), 19759–19770 (2013).

[5] R. D. Robinson, B. Sadtler, D. O. Demchenko, C. K. Erdonmez, L. W. Wang, and A. P. Alivisatos, "Spontaneous superlattice formation in nanorods through partial cation exchange," Science **317**(5836), 355–358 (2007).

[6] D. H. Son, S. M. Hughes, Y. Yin, and A. Paul Alivisatos, "Cation exchange reactions in ionic nanocrystals," Science **306**(5698), 1009–1012 (2004).

[7] A. Nelson, S. Honrao, R. G. Hennig, and R. D. Robinson, "Nanocrystal symmetry breaking and accelerated solid-state diffusion in the lead–cadmium sulfide cation exchange system," Chem. Mater. **31**(3), 991–1005 (2019).

[8] S. L. White, J. G. Smith, M. Behl, and P. K. Jain, "Co-operativity in a nanocrystalline solid-state transition," Nat. Commun. **4**(1), 2933 (2013).

[9] S. L. White, P. Banerjee, I. Chakraborty, and P. K. Jain, "Ion exchange transformation of magic-sized clusters," Chem. Mater. **28**(22), 8391–8398 (2016).

[10] J. L. Stein, M. I. Steimle, M. W. Terban, A. Petrone, S. J. L. Billinge, X. Li, and B. M. Cossairt, "Cation exchange induced transformation of InP magic-sized clusters," Chem. Mater. **29**(18), 7984–7992 (2017).

[11] J. Yang, F. Muckel, W. Baek, R. Fainblat, H. Chang, G. Bacher, and T. Hyeon, "Chemical synthesis, doping, and transformation of magic-sized semiconductor alloy nanoclusters," J. Am. Chem. Soc. **139**(19), 6761–6770 (2017).

[12] L. He, C. Luan, S. Liu, M. Chen, N. Rowell, Z. Wang, Y. Li, C. Zhang, J. Lu, M. Zhang, B. Liang, and K. Yu, "Transformations of magic-size clusters via precursor compound cation exchange at room temperature," J. Am. Chem. Soc. **144**(41), 19060–19069 (2022).

[13] F. Muckel, J. Yang, S. Lorenz, W. Baek, H. Chang, T. Hyeon, G. Bacher, and R. Fainblat, "Digital doping in magic-sized CdSe clusters," ACS Nano **10**(7), 7135–7141 (2016).

[14] H. Han, Y. Yao, A. Bhargava, Z. Wei, Z. Tang, J. Suntivich, O. Voznyy, and R. D. Robinson, "Tertiary hierarchical complexity in assemblies of sulfur-bridged metal chiral clusters," J. Am. Chem. Soc. **142**(34), 14495–14503 (2020).

[15] M. S. Bootharaju, W. Baek, G. Deng, K. Singh, O. Voznyy, N. Zheng, and T. Hyeon, "Structure of a subnanometer-sized semiconductor $Cd_{14}Se_{13}$ cluster," Chem **8**(11), 2978–2989 (2022).

[16] D. C. Gary, S. E. Flowers, W. Kaminsky, A. Petrone, X. Li, and B. M. Cossairt, "Single-crystal and electronic structure of a 1.3 nm indium phosphide nanocluster," J. Am. Chem. Soc. **138**(5), 1510–1513 (2016).

[17] J. E. Denhardt and K. R. Kittilstved, "Core-doped $[(Cd_{1-x}Co_x)_{10}S_4(SPh)_{16}]^{4-}$ clusters from a self-assembly route," Inorg. Chem. **60**(20), 15270–15277 (2021).

[18] J. Yang, F. Muckel, B. K. Choi, S. Lorenz, I. Y. Kim, J. Ackermann, H. Chang, T. Czerney, V. S. Kale, S.-J. Hwang, G. Bacher, and T. Hyeon, "Co^{2+}-doping of magic-sized CdSe clusters: Structural insights via ligand field transitions," Nano Lett. **18**(11), 7350–7357 (2018).

[19] D. R. Nevers, C. B. Williamson, T. Hanrath, and R. D. Robinson, "Surface chemistry of cadmium sulfide magic-sized clusters: A window into ligand-nanoparticle interactions," Chem. Commun. **53**(19), 2866–2869 (2017).

[20] W. Jiang, Z. Wu, X. Yue, S. Yuan, H. Lu, and B. Liang, "Photocatalytic performance of Ag_2S under irradiation with visible and near-infrared light and its mechanism of degradation," RSC Adv. **5**(31), 24064–24071 (2015).

[21] T. Y. Liang, S. J. Chan, A. S. Patra, P.-L. Hsieh, Y.-A. Chen, H.-H. Ma, and M. H. Huang, "Inactive Cu_2O cubes become highly photocatalytically active with Ag_2S deposition," ACS Appl. Mater. Interfaces **13**(9), 11515–11523 (2021).

[22] C. Wang, Y. Wang, L. Xu, D. Zhang, M. Liu, X. Li, H. Sun, Q. Lin, and B. Yang, "Facile aqueous-phase synthesis of biocompatible and fluorescent Ag_2S nanoclusters for bioimaging: Tunable photoluminescence from red to near infrared," Small **8**(20), 3137–3142 (2012).

[23] G. B. Hoflund, J. F. Weaver, and W. S. Epling, "Ag foil by XPS," Surf. Sci. Spectra **3**, 151–156 (1994).

[24] I. Z. Gutierrez, C. Gerke, Y. Shen, E. Ximendes, M. M. Silvan, R. Marin, D. Jaque, O. G. Calderón, S. Melle, and J. Rubio-Retama, "Boosting the near-infrared emission of Ag_2S nanoparticles by a controllable surface treatment for bioimaging applications," ACS Appl. Mater. Interfaces **14**(4), 4871–4881 (2022).

[25] N. Nair and B. R. Sankapal, "Cationic-exchange approach for conversion of two dimensional CdS to two dimensional Ag_2S nanowires with an intermediate core–shell nanostructure towards supercapacitor application," New J. Chem. **40**(12), 10144–10152 (2016).

[26] M. Ristova and M. Ristov, "XPS profile analysis on CdS thin film modified with Ag by an ion exchange," Appl. Surf. Sci. **181**, 68–77 (2001).

[27] E. G. Durmusoglu, M. M. Yildizhan, M. A. Gulgun, and H. Yagci Acar, "Production of small, stable PbS/CdS quantum dots via room temperature cation exchange followed by a low temperature annealing processes," J. Phys. Chem. C **121**(45), 25520–25530 (2017).

[28] P. Thakur, S. S. Joshi, and K. R. Patil, "Investigations of CdS and Ag–CdS nanoparticles by X-ray photoelectron spectroscopy," Appl. Surf. Sci. **257**(5), 1390–1394 (2010).

[29] X. Cheng, M. Liu, A. Zhang, S. Hu, C. Song, G. Zhang, and X. Guo, "Size-controlled silver nanoparticles stabilized on thiol-functionalized MIL-53(Al) frameworks," Nanoscale **7**(21), 9738–9745 (2015).

[30] C. H. M. van Oversteeg, F. E. Oropeza, J. P. Hofmann, E. J. M. Hensen, P. E. de Jongh, and C. de Mello Donega, "Water-dispersible copper sulfide nanocrystals via ligand exchange of 1-dodecanethiol," Chem. Mater. **31**(2), 541–552 (2019).

[31] Y. Xie, A. Riedinger, M. Prato, A. Casu, A. Genovese, P. Guardia, S. Sottini, C. Sangregorio, K. Miszta, S. Ghosh, T. Pellegrino, and L. Manna, "Copper sulfide nanocrystals with tunable composition by reduction of covellite nanocrystals with Cu^+ ions," J. Am. Chem. Soc. **135**(46), 17630–17637 (2013).

[32] R. G. Goel and N. K. Jha, "Triphenylphosphine complexes of cadmium(II) perchlorate, nitrate, and trifluoroacetate preparation, characterization, and spectral studies," Can. J. Chem. **59**(23), 3267–3272 (1981).

[33] K. E. Hughes, K. H. Hartstein, and D. R. Gamelin, "Photodoping and transient spectroscopies of copper-doped CdSe/CdS nanocrystals," ACS Nano **12**(1), 718–728 (2018).